NMR structure of the N-terminal domain of *E. coli* DnaB helicase: implications for structure rearrangements in the helicase hexamer

Johan Weigelt[1], Susan E Brown[2], Caroline S Miles[2†], Nicholas E Dixon[2] and Gottfried Otting[1*]

Background: DnaB is the primary replicative helicase in *Escherichia coli*. Native DnaB is a hexamer of identical subunits, each consisting of a larger C-terminal domain and a smaller N-terminal domain. Electron-microscopy data show hexamers with C_6 or C_3 symmetry, indicating large domain movements and reversible pairwise association.

Results: The three-dimensional structure of the N-terminal domain of *E. coli* DnaB was determined by nuclear magnetic resonance (NMR) spectroscopy. Structural similarity was found with the primary dimerisation domain of a topoisomerase, the gyrase A subunit from *E. coli*. A monomer–dimer equilibrium was observed for the isolated N-terminal domain of DnaB. A dimer model with C_2 symmetry was derived from intermolecular nuclear Overhauser effects, which is consistent with all available NMR data.

Conclusions: The monomer–dimer equilibrium observed for the N-terminal domain of DnaB is likely to be of functional significance for helicase activity, by participating in the switch between C_6 and C_3 symmetry of the helicase hexamer.

Addresses: [1]Department of Medical Biochemistry and Biophysics, Karolinska Institutet, S-171 77 Stockholm, Sweden and [2]Centre for Molecular Structure and Function, Research School of Chemistry, Australian National University, Canberra ACT 0200, Australia.

[†]Present address: Department of Chemistry, University of Edinburgh, Edinburgh EH9 3JJ, Scotland, UK.

*Corresponding author.
E-mail: Gottfried.Otting@mbb.ki.se

Key words: DnaB, helicase, NMR

Received: 28 January 1999
Revisions requested: 25 February 1999
Revisions received: 1 March 1999
Accepted: 5 March 1999

Published: 1 June 1999

Structure June 1999, 7:681–690
http://biomednet.com/elecref/0969212600700681

 ISSN 0969-2126

Introduction

Helicases are enzymes that separate duplex DNA or RNA into single strands with the help of ATP. They are involved in fundamental reactions involving DNA and RNA, including replication, repair and recombination, as well as transcription and translation [1,2]. Defective helicase genes are increasingly found to be at the basis of inheritable human disease [3]. Recently, crystal structures have been determined for helicases belonging to superfamilies I, II and III [4–7], but their functional mechanism is still poorly understood [8]. All three helicases crystallised as monomers. No structure of an intact hexameric helicase has yet been reported, although crystallisation reports have been published for the plasmid RSF1010 RepA protein [9] and the helicase domain of bacteriophage T7 gene 4 protein (gp4) [10]. Furthermore, the structure of the RNA-binding domain of the hexameric *Escherichia coli* rho transcription factor has been determined [11,12].

DnaB is the most extensively studied helicase among the hexameric helicases, and it is a key replication protein in *E. coli* [13]. It is one of about twenty different proteins that constitute the bacterial replisome, a nucleoprotein complex that accomplishes DNA synthesis at replication forks during the duplication of the bacterial chromosome [14]. At replication initiation, DnaB is loaded onto DNA by interactions with both DnaA and DnaC proteins [15–17]. Driven by ATP hydrolysis, the DnaB helicase unwinds duplex DNA into single strands [18]. This allows DNA polymerase III to copy the single-stranded DNA template [19]. As well as binding dNTPs, rNTPs [13] and single-stranded DNA [19], DnaB interacts with other replication proteins including DnaC [20], DnaG primase [18,21] and the τ subunit of DNA polymerase III [22].

Functional DnaB is composed of six identical 52 kDa subunits [23]. Proteolytic studies indicated that each subunit consists of two domains, a smaller N-terminal and a larger C-terminal domain. Both domains are required for helicase function [24,25]. Furthermore, ATPase and DNA-binding activities were found to be located in the C-terminal domain, whereas the smaller N-terminal domain is important for hexamerisation [24,25].

Single crystals have been obtained for DnaB, but they did not diffract satisfactorily (N Dammerova, CSM, NED and DL Ollis, unpublished results). Electron-microscopy (EM) studies of DnaB and related hexameric helicases revealed a symmetric arrangement into a ring structure with a pore diameter of about 3–4 nm [26,27]. Depending on the sample conditions, DnaB hexamer particles were observed with sixfold (C_6) and threefold (C_3) symmetry

Figure 1

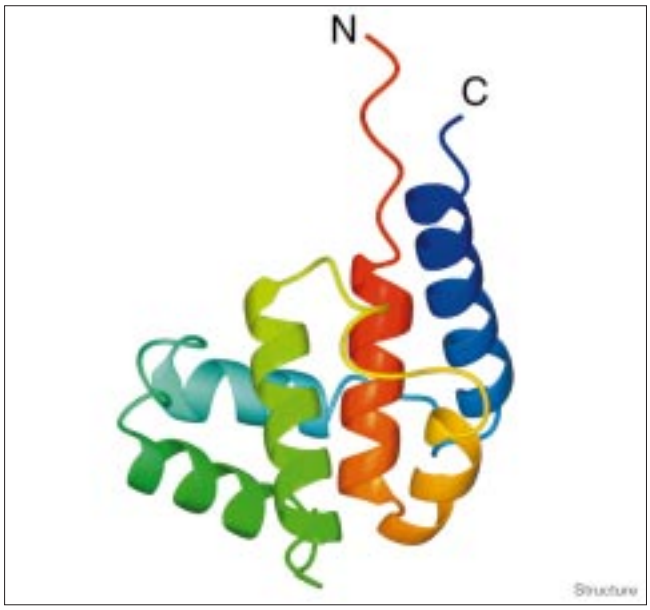

Ribbon diagram of the conformer closest to the mean structure of DnaB(24–136), displaying the six main helical segments.

[28] together with species of intermediate appearance [27]. The interconversion between different conformations of the DnaB hexamer has been proposed to be of functional significance [27,29].

Here, we report the three-dimensional solution structure of the N-terminal domain of DnaB, comprising residues 24–136. Previous nuclear magnetic resonance (NMR) spectroscopy studies on DnaB N-terminal fragments (consisting of residues 1–142 and 1–161) identified the flexible regions of the domain, mapped the structured core to residues 24–136 [30] and delineated the secondary structure [31]. The present NMR structure is the first structure at atomic resolution of a domain from a DnaB helicase. The monomer–dimer equilibrium reported here for the N-terminal DnaB domain in solution supports the presence of an association–dissociation equilibrium for this domain in the DnaB hexamer, as proposed previously from EM data [29].

Results and discussion

Structure of the N-terminal domain of DnaB

The structure of the N-terminal domain of DnaB, DnaB(24–136), was determined in aqueous solution at pH 7.5, 32°C, using protein concentrations of about 2.3 mM. A proportion of the protein was dimeric under these conditions, resulting in an effective rotational correlation time of 10 ns [32]. Three weak intermolecular nuclear Overhauser effects (NOEs) were identified in the course of the analysis. Recording of a two-dimensional (2D) ^{13}C-edited-^{13}C-filtered nuclear Overhauser effect spectroscopy (NOESY) spectrum [33,34] with a 1:1 mixture of unlabelled and uniformly ^{13}C/^{15}N (u-^{13}C/^{15}N) labelled protein was attempted, but the sensitivity of the experiment was insufficient for the detection of the intermolecular NOEs. Consequently, all but three distance restraints were interpreted as arising from a monomer. The relative orientations of the helices in the resulting NMR structure were verified by dipolar coupling constants measured at low concentration (0.1 mM). Thus, only the orientation of the surface sidechains at the dimer interface could be affected by a confusion of intramolecular and intermolecular distance restraints.

The NMR structure of DnaB(24–136) (Figures 1,2) consists of six α helices (Figure 3), with a 3_{10} helical segment at the N terminus of helix 2 (residues 44–46). In addition, the structure contains two helical turns, comprising residues 56–58 and 97–99. The hydrophobic core of the protein is centred around the C-terminal end of helix 1, which is completely buried. Charged amino acid sidechains are distributed evenly on the protein surface and are easily accessible to the solvent (Figure 4). The only exceptions are the sidechains of Glu33 and Glu70. Although the sidechain oxygens of Glu70 are still solvent-exposed, their main hydrogen-bonding partners seem to be Ser89 H^{γ} and Asn93 $H^{\varepsilon 21}$. The sidechain of Glu33, which is one of the few fully conserved residues among DnaBs (Figure 3), is completely buried. In the NMR structure of DnaB(24–136), Glu33 $O^{\varepsilon 1}$ hydrogen bonds to $H^{\delta 1}$ of the highly conserved His64. The presence of this hydrogen bond is documented by NOEs between Glu33 $C^{\beta}H_2$ and His64 $H^{\delta 1}$, and the downfield shift of the ^{1}H NMR signal of His64 $H^{\delta 1}$ (14.9 ppm). The ^{1}H chemical shifts of the carbon-bound protons $H^{\varepsilon 1}$ and $H^{\delta 2}$ of His64 suggest that the histidine sidechain is uncharged, in agreement with the formation of a hydrogen bond rather than a salt bridge. Buried charged carboxyl groups with hydrogen bonds to histidine sidechains are a common feature of serine proteases and also occur as a structural motif in nonproteolytic proteins [35].

The NMR structure of DnaB(24–136) is well-defined for residues 30–134. The H^N resonances of six residues in loop regions and at the N terminus could not be observed (Figure 3), affecting the definition of those segments (Figure 2b). The 23 N-terminal residues of DnaB have previously been found to be highly flexible [30], in agreement with rapid cleavage of the 14 N-terminal residues in proteolysis experiments of full-length DnaB [24]. The linker region between the N- and C-terminal domains of DnaB has a high α-helical propensity in secondary-structure predictions [36], but it was found to be disordered in the DnaB(1–161) fragment studied earlier by NMR [30].

Sequence conservation of DnaB N-terminal domains

A sequence comparison between DnaB N-terminal domains from different organisms shows only four completely conserved residues (Figure 3). Yet a conserved

Figure 2

Different stereo representations of the NMR solution structure of DnaB(24–136). All three representations show the structure in the same orientation as in Figure 1. (a) Backbone trace of the conformer closest to the mean structure. (b) Ensemble of 20 conformers, using the backbone atoms of residues 29–134 for superposition. (c) Heavy-atom display of the conformer closest to the mean structure. The protein backbone is drawn as a thick grey line. Hydrophobic sidechains (Ala, Phe, Ile, Leu, Met, Pro, Val, Trp) are drawn in yellow, polar sidechains (Asn, Gln, Ser, Thr, Tyr, His) are drawn in magenta, positively (Lys and Arg) and negatively (Asp and Glu) charged sidechains are coloured blue and red, respectively.

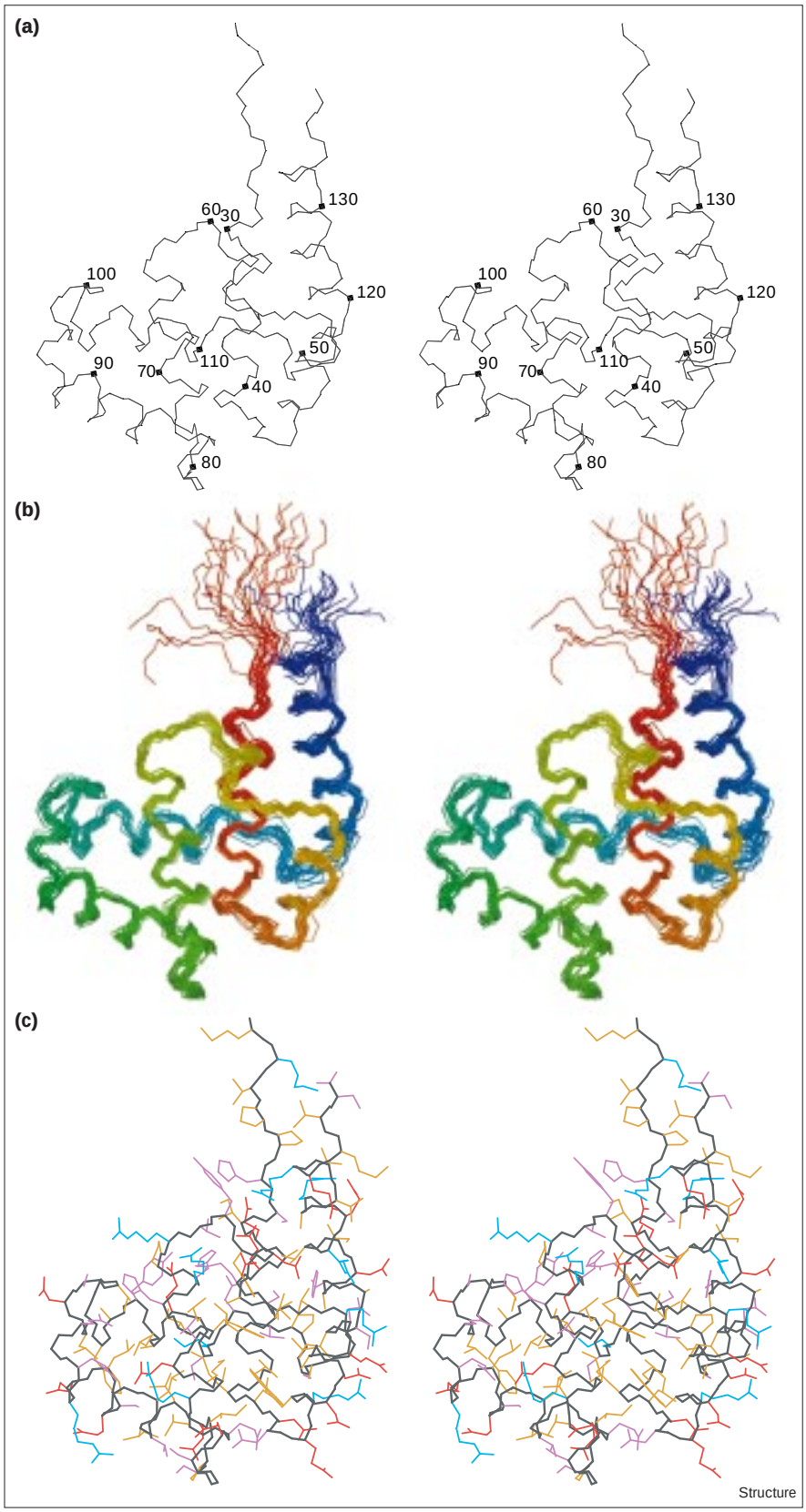

Figure 3

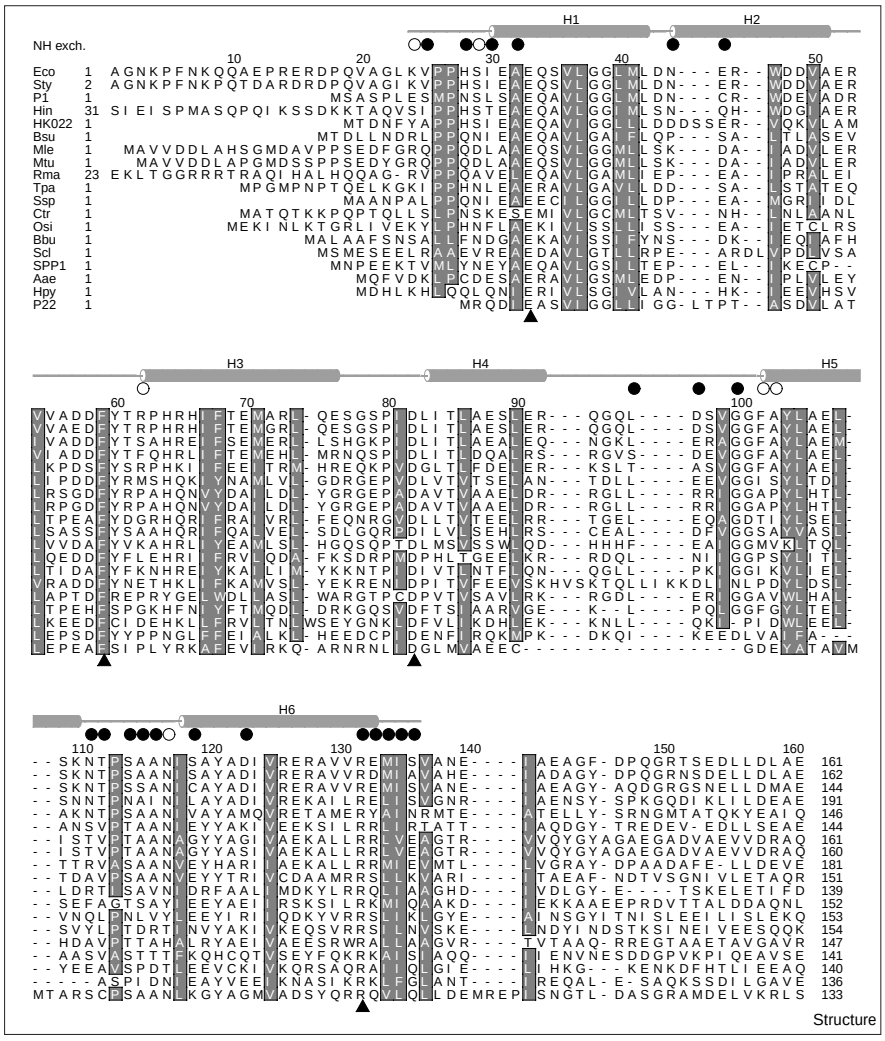

Sequence alignment of the N-terminal portions of 19 DnaB-like helicases from different species. Eco (*Escherichia coli*, SwissProt P03005, present study), Sty (*Salmonella typhimurium*, PIR A32011), P1 (bacteriophage P1, EMBL AJ011592), Hin (*Haemophilus influenzae*, SwissProt P45256), HK022 (bacteriophage HK022, PIR S3527), Bsu (*Bacillus subtilis*, SwissProt P37469), Mle (*Mycobacterium leprae*, SwissProt P46394), Mtu (*Mycobacterium tuberculosis*, SwissProt P71715), Rma (*Rhodothermus marinus*, EMBL Y13813), Tpa (*Treponema pallidum*, GenBank 3322317), Ssp (*Synechocystis* PCC6803, SwissProt Q55418), Ctr (*Chlamydia trachomatis*, GenBank 3328934), Osi (*Odontella sinensis*, SwissProt P49519), Bbu (*Borrelia burgdorferi*, GenBank 2687992), Scl (*Streptomyces clavuligerus*, GenBank 581632), SPP1 (bacteriophage SPP1, GenBank 2764919), Aae (*Aquifex aeolicus*, GenBank 2983861), Hpy (*Helicobacter pylori*, SwissProt O25916), P22 (bacteriophage P22, SwissProt P03006). Shaded boxes mark hydrophobic or aromatic (except His) residues that are conserved in at least 17 of the sequences. Residues conserved in all 19 sequences are identified by triangles. The secondary structure of DnaB(24–136) is indicated at the top; the α helices are represented by cylinders. Filled circles mark residues with H^N protons in fast exchange with the solvent, identified from exchange cross peaks with the water resonance in a 2D ROE-^{15}N-HSQC experiment. Open circles indicate residues for which the H^N resonance could not be observed.

three-dimensional structure is indicated by the fact that almost all highly conserved hydrophobic residues are buried (Figure 4), as expected for structurally important residues. The solvent-exposed, but conserved, hydrophobic residues

Figure 4

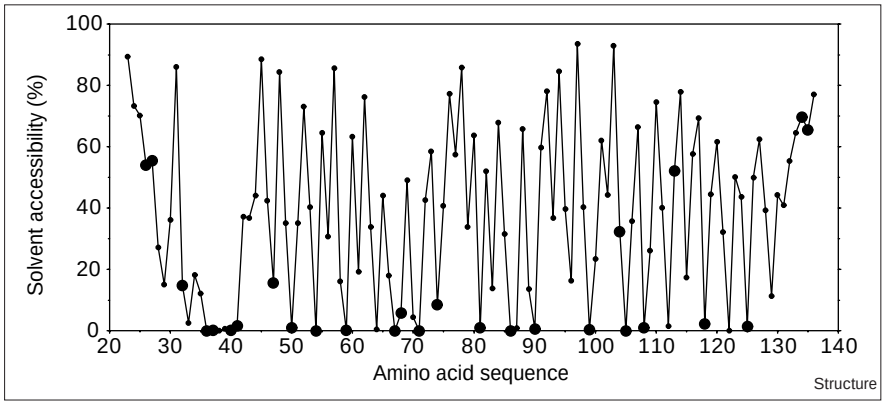

Solvent accessibilities of the amino acid sidechains in DnaB(24–136) as a percentage of their calculated accessibilities if they were located in a hypothetical poly-Gly α helix with a fully extended sidechain [71]. The values were averaged over the 20 NMR conformers. Large filled circles identify the conserved hydrophobic residues from Figure 3.

Pro27, Pro28, Met134 and Ile135 may be important for interactions with either the C-terminal domain or other proteins involved in the replication complex. Pro113 is located in the least well-defined loop of the structure. The conservation of Tyr104, although it is in close proximity to the dimerisation interface (see below), may be of lesser significance, as it is not very solvent-exposed.

Of the four totally conserved residues, only mutations of Asp82 have been studied. The D82N mutation of the *Salmonella typhimurium* DnaB helicase, which is closely related to the *E. coli* protein (Figure 3), has been shown to impair helicase function [37]. The function of this residue is unclear, except that its negative charge combined with its location at the N-terminal end of helix 4 probably contributes to the stability of this helix. Similarly, the positive charge of Arg132 may contribute to the stability of helix 6 and/or be involved in protein–protein interactions, as the mutations I135N, I141T and L156P in the linker between the N- and C-terminal domains have been shown to interfere with helicase function [38].

Structure of dimeric DnaB N-terminal domain

A model of dimeric DnaB(24–136) was built on the basis of concentration-dependent chemical shifts (Figure 5), intermolecular NOEs and residual dipolar coupling constants measured in a liquid-crystalline phase. Chemical shift changes preferentially mapped onto a single face of the N-terminal domain, which is comprised of helices 4 and 5 and the connecting loop (Figure 6). Three intermolecular NOEs were identified between Ile84 $C^{\gamma 2}H_3$ and Ala106 $C^{\beta}H_3$, between Glu88 $C^{\gamma}H_2$ and Ala103 $C^{\beta}H_3$, and between Glu88 $C^{\gamma}H_2$ and Ala103 $C^{\alpha}H$. These NOEs are readily explained by a symmetric dimer and cannot be interpreted as intramolecular NOEs, because the respective protons are too far apart in the monomeric structure.

Figure 7a shows a model of the dimer of DnaB(24–136) that is in agreement with all available data. In particular, it agrees with the residual dipolar ^1H–^{15}N coupling constants measured in a liquid-crystalline phase at 0.1 mM and 1.1 mM protein concentration. The dipolar couplings measured at high protein concentration merely corresponded to an increased order parameter compared to the measurements at low protein concentration, resulting in a uniform increase of the dipolar couplings independent of the orientation of the N–H vectors. This observation is readily

Figure 5

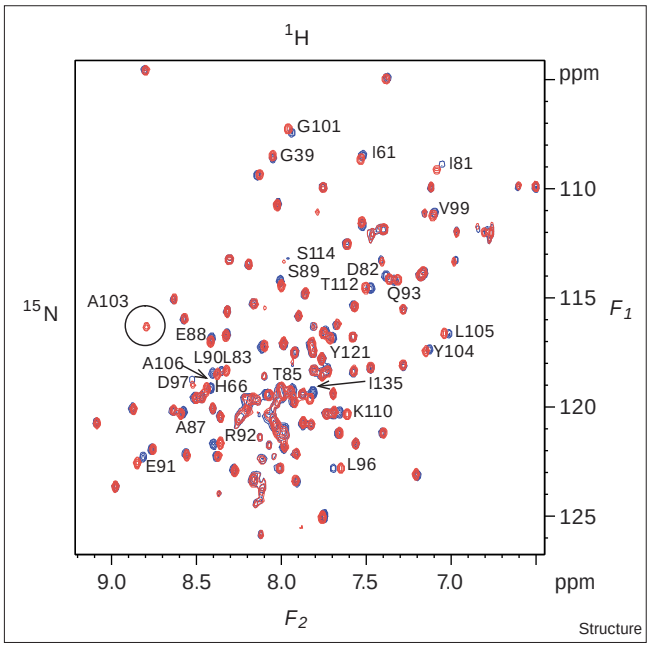

Overlay of ^{15}N–^1H HSQC spectra of DnaB(24–136) measured under identical conditions at protein concentrations of 0.1 mM (red) and 2 mM (blue). Cross peaks displaying concentration-dependent chemical shifts of at least 5 Hz and/or 10 Hz in the ^{15}N and ^1H dimension, respectively, are identified with their assignments. The open circle identifies the amide cross peak of Ala103 visible only at protein concentrations below 0.45 mM.

Figure 6

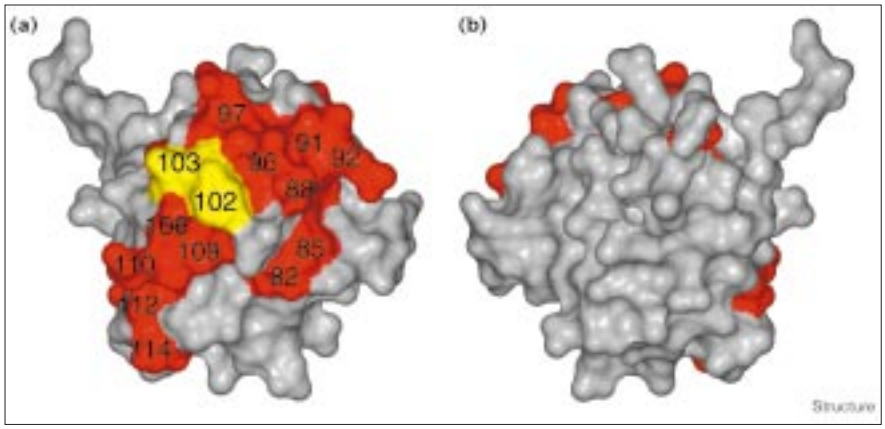

Surface representation of DnaB(24–136) showing (a) the dimerisation interface and (b) the opposite side of the molecule obtained by a 180° rotation about a vertical axis. Residues for which significant concentration-dependent amide chemical shifts were identified (Figure 5) are coloured in red. Phe102 and Ala103, for which the H^N resonances were not observed at high protein concentration, are located in the middle of the dimerisation interface (yellow).

explained by the fact that the long axis of the orientational tensor in the dimer (horizontal in Figure 7a) is close to the corresponding experimentally determined tensor axis in the monomer. Any significant change in direction of the long tensor axis between monomer and dimer would have scaled the dipolar couplings differently for different helices.

Only a single set of resonances was observed, indicating that the dimer is in rapid equilibrium with the monomer. The dissociation constant could not be determined by NMR, as the chemical shift changes were virtually linear over the entire concentration range studied. Analytical-ultracentrifugation experiments at pH 6.6 suggested a dissociation constant in the low millimolar range (data not shown). The dimer interface buries about 600 Å^2 of solvent-accessible surface area in a hydrophobic core flanked by polar residues. The amide resonances of Phe102, which is at the centre of the interface, and of Ala103 could not be observed at high protein concentration; however, at low concentration the Ala103 amide resonance could be identified (Figure 5). This indicates that the dimer interface is dynamic in nature, resulting in selective exchange broadening of these amide-proton resonances.

Homology with the primary dimerisation domain of *E. coli* gyrase A

A search of the Protein Data Bank (PDB) using the program DALI [39] identified the primary dimerisation domain of *E. coli* gyrase A [40] as the protein most closely related to DnaB(24–136) (Z score 3.1, 2.8 Å root mean square deviation (rmsd) for 73 superimposed Cα atoms). The dimer of this gyrase A domain is shown in Figure 7b. Although the dimer has overall dimensions similar to those of DnaB(24–136), the dimer structures differ largely at the dimer interface, which is more extended in the gyrase. A direct comparison between the monomeric domains of DnaB(24–136) and gyrase A show that structural homologies are almost exclusively in the regions that are remote from the interface (Figure 8). A similar situation has been observed for the corresponding dimerisation domain of yeast type II topoisomerase [41], which has a different dimerisation interface from that of

Figure 7

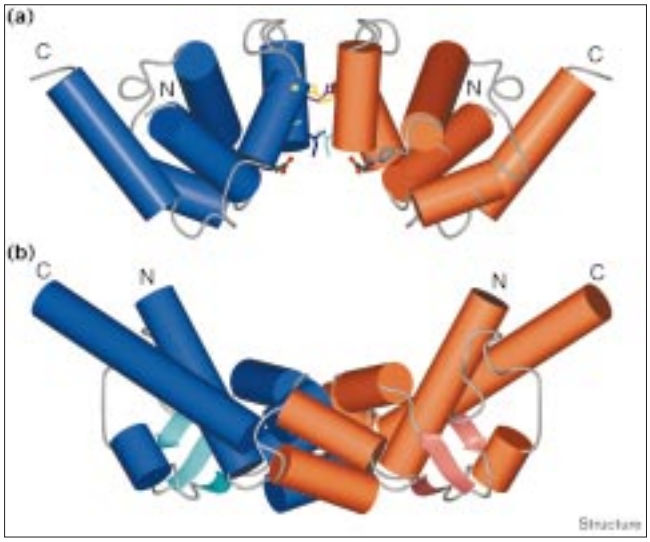

Dimerisation domains from DnaB and gyrase A. Helices are represented by cylinders and β sheets by ribbons. (a) Model of the symmetric dimer of the N-terminal domain of DnaB. The sidechains of the amino acids involved in intermolecular NOEs (Ile84, Glu88, Ala103 and Ala106) are shown in stick representation, with equal colours for both partners involved in an intermolecular NOE. The totally conserved residue Asp82 is shown in ball-and-stick representation. (b) The primary dimerisation domain of gyrase A [40].

Figure 8

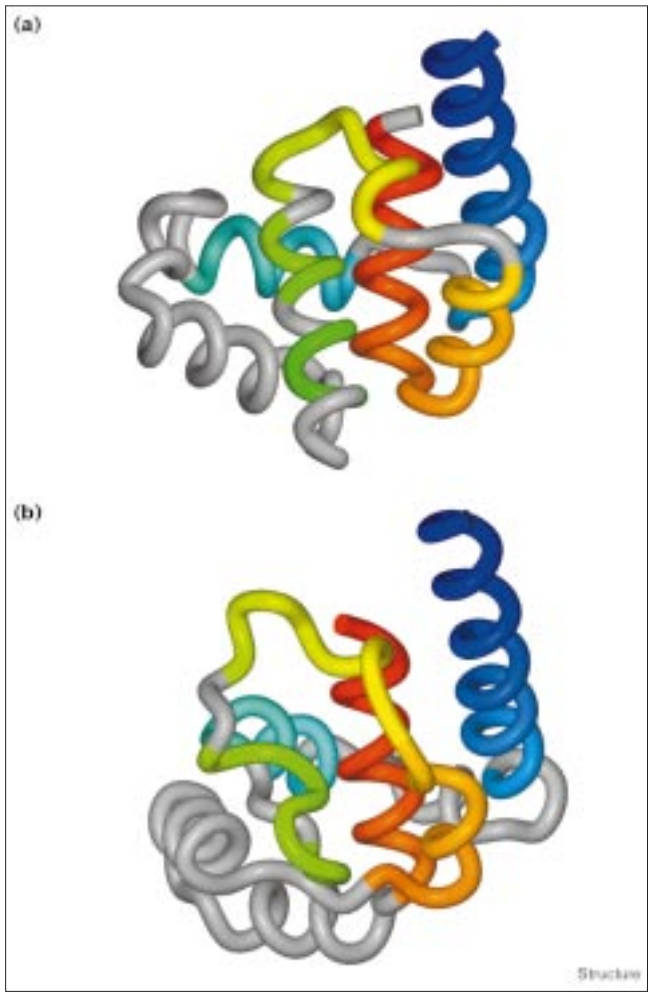

Comparison of the overall fold between (a) the N-terminal domain of *E. coli* DnaB and (b) the primary dimerisation domain of *E. coli* gyrase A. Only the protein backbones are shown, omitting the poorly defined N- and C-terminal residues of DnaB(24–136). The orientation of the DnaB domain is the same as that used in Figure 1. The parts of the molecules that were identified as being structurally homologous by the program DALI [39] are colour-coded in the same way as in Figure 1.

gyrase A, with the more remote parts of the domain being conserved [40].

Comparison with electron-microscopy data

EM studies of DnaB show that the hexamer can exist in states with both threefold (C_3) and sixfold (C_6) symmetry [26–28]. Simple structural models proposed for these states (Figure 9) differ by a large displacement of the smaller one of the two domains in each subunit of the hexamer, leading to a trimer of dimers with pairwise-associated small domains in the C_3 state. The small domains are independent from each other in the C_6 state [27], which cannot, by definition, contain symmetrical subunit (or domain) dimers. The NMR structure of DnaB(24–136) shows that the N-terminal domain of DnaB is globular, supporting its identification with the small domain in the hexamer models suggested from EM studies [26,29]. The larger domain in the hexamer models has previously been identified with the C-terminal domain [26], which is supported by shared amino acid sequence motifs with helicase domains that are structurally homologous to hexameric RecA and F1 ATPase [12,42]. Most interestingly, the monomer–dimer equilibrium experimentally observed for the isolated N-terminal domain in solution matches the association–dissociation equilibrium of the small domains in the C_6–C_3 conversion suggested by EM data. The present data provide the first evidence of how the N-terminal domain, by providing a dimerisation interface, might stabilise one form of the DnaB hexamer and participate in its conformational transitions, which may be a prerequisite for helicase activity.

Interaction with single-stranded DNA, DnaC, magnesium and ATP

Association of DnaB(24–136) with single-stranded DNA (dT_{16}), DnaC, Mg^{2+} and ATP was probed by monitoring the amide chemical shifts of DnaB(24–136) in ^{15}N heteronuclear single-quantum correlation (^{15}N-HSQC) spectra with and without these compounds. Mg^{2+} showed weak, nonspecific interactions at all sites near negatively charged sidechains. No interactions were observed with ATP, DnaC or with dT_{16}. If the N-terminal domain of DnaB interacts with DnaC, as has been suggested [24], additional stabilising interaction sites must exist in the C-terminal domain, the linker region, or the flexible N-terminal region (residues 1–23).

Figure 9

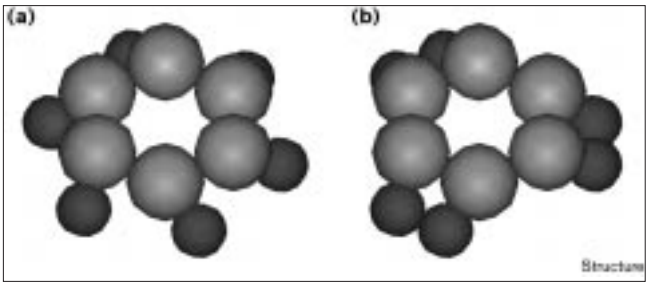

Models of two different hexameric states of the *E. coli* DnaB helicase [29]. The smaller and larger domain are proposed to be identical to the N-terminal and C-terminal domains, respectively. (a) Hexamer with C_6 symmetry. (b) Hexamer with C_3 symmetry and pairwise-associated N-terminal domains. The twofold symmetry suggested by the model for each pair of subunits is not observed experimentally [29]; although the N-terminal domains may associate in a symmetric fashion, the sixfold symmetry of the C-terminal domains is broken in this hexameric state.

Biological implications

Helicases are key enzymes in DNA metabolism and defective genes for these proteins are the cause of a number of inherited human diseases. In spite of a large body of biochemical data, their mechanism of action is still not understood.

DnaB is the primary replicative helicase in *E. coli*, unwinding duplex DNA into single strands during replication. DnaB is a hexamer composed of identical subunits, each consisting of a larger C-terminal and a smaller N-terminal domain. Here, we report the solution structure of the N-terminal domain, which is required for helicase activity. This is the first high-resolution structure of a DnaB domain.

Electron microscopy studies of DnaB showed that the hexamer can exist in states with both threefold (C_3) and sixfold (C_6) symmetry. Simple structural models proposed for these states differ by a large displacement of the smaller of the two domains in each subunit of the hexamer in an association–dissociation equilibrium. The globular appearance of the N-terminal domain suggests that it is identical to the small domain in the hexamer models. The putative dimerisation of the small domains in the C_6–C_3 conversion is supported by the monomer–dimer equilibrium experimentally observed for the isolated N-terminal domain in solution. The dimer structure shares similarities with the primary dimerisation domain of type II topoisomerases; this dimerisation domain is thought to function as a gate for the release of double-stranded DNA. The NMR structure of the dimeric N-terminal domain provides a basis for mutational studies to analyse the functional significance of the C_6–C_3 conversion in hexameric DnaB.

Materials and methods

Construction of plasmid pSB955 for the overexpression of DnaB(24–136)

Plasmid pSB955 was generated using a polymerase chain reaction (PCR) strategy with plasmid pCM860 [30] as template. Two primers were designed, the first (5′-GAAGGAGATATACATATGAAAGTGCCTC-CGCACTCG-3′) to insert an *Nde*I restriction site at a new ATG start codon before codon 24 of *dnaB*, and the second (5′-CTCGAATTCT-TACGAGATCATCTCACGGACAACGGCACG-3′) to insert a TAA stop codon followed by an *Eco*RI restriction site immediately after the serine 136 codon. The PCR reaction mixture (50 μl) contained template plasmid pCM860 (77 ng or 77 pg), both primers (1 μM each), $MgSO_4$ (varying between 2 and 9 mM), all four dNTPs (1 μM each), Vent DNA polymerase

(1 unit, New England Biolabs) and manufacturer supplied buffer for Vent DNA polymerase. The thermal cycler was programmed as follows: 94°C for 5 min; 94°C for 30 s, 55°C for 1 min and 72°C for 1 min (32 times); 72°C for 20 min; and 4°C for 5 min. The amplified DNA (371 bp) was concentrated using a Wizard PCR prep (Promega), and purified from a 1.5% agarose gel using a QIAEX II kit (QIAGEN). The purified DNA was digested with NdeI and EcoRI, and ligated using T4 ligase to the 4642 bp *Nde*I–*Eco*RI fragment of pETMCSI [30], which is a derivative of pET3c [43]. Ampicillin-resistant transformants of BL21(DE3) were selected at 37°C and plasmid DNA (4991 bp) was isolated on a small scale using a Bresaspin mini-prep (Bresatec). Overproduction of the desired 12 kDa protein at 37°C was confirmed by sodium dodecyl sulphate polyacrylamide gel electrophoresis (SDS–PAGE). The sequence of *dnaB* from the selected plasmid pSB955 was confirmed by amplification of the DNA using an ABI PRISM dye terminator sequencing kit and subsequent analysis using an Applied Biosystems 373A sequencer.

Protein overproduction and purification

Strain BL21(DE3)/pLysS/pSB955 was used to prepare unlabelled, u-^{15}N-labelled, u-^{13}C/^{15}N-labelled and 10%-^{13}C/u-^{15}N-labelled DnaB(24–136). All culture media were supplemented with 50 μg/ml ampicillin and 50 μg/ml chloramphenicol. Cells for production of unlabelled DnaB(24–136) were grown in 250 or 500 ml of LB medium supplemented with 25 μg/ml thymine. Labelled proteins were prepared from cultures of 100 or 250 ml of minimal medium, consisting of 1.5 g/l $^{15}NH_4Cl$ (Novachem or Cambridge Isotope Laboratories), 100 mM Na/K phosphate buffer, trace salts, 1 μg/ml vitamin B1, 1 mM $MgSO_4$ and appropriate amounts of glucose (40 mM D(+)-glucose for ^{15}N- labelled protein, or 20 mM [$^{13}C_6$]-D(+)-glucose (Cambridge Isotope Laboratories) for ^{13}C-labelled proteins). All cultures were grown at 37°C until the absorbence at 595 nm reached 0.5. Protein production was induced by the addition of isopropyl-β-D-thiogalactoside (IPTG) to 1 mM and the cells were grown for a further four hours. To prepare the 10%-^{13}C/u-^{15}N labelled protein, 200 mM unlabelled D(+)-glucose was added to the 100 ml culture immediately prior to addition of IPTG [44].

Cells were harvested by centrifugation, resuspended in lysis buffer (50 mM TRIS-HCl pH 7.6, 10% w/v sucrose, 100 mM NaCl, 2 mM DTT, 10 mM spermidine-Cl; 15 ml/g cells) and lysed using a French Press. The lysate was clarified by centrifugation, and the proteins in the supernatant were precipitated using 0.4 g/ml ammonium sulfate. The pellets obtained after centrifugation were resuspended in a few millilitres of buffer A (50 mM TRIS-HCl pH 7.6, 20% v/v glycerol, 5 mM $MgCl_2$) and dialysed overnight in the same buffer.

All DnaB(24–136) protein samples were purified at 4°C using anion-exchange (DEAE Fractogel, Merck) and gel-filtration (Sephadex G-50, Pharmacia) chromatography following the procedure in [30], except that the protein was precipitated using 0.4 g/ml ammonium sulfate, and the final dialysis buffer D was 20 mM potassium phosphate pH 6.5. DnaB and DnaC were overproduced simultaneously as described previously [23,45], and purified initially by anion-exchange chromatography (DEAE Fractogel) [28]. DnaB was further purified on a hydroxyapaptite column (BioRad) [28]. DnaC was eluted in a NaCl gradient from a phosphocellulose (P11, Whatman) column in a buffer containing 25 mM sodium phosphate pH 7.1, 1 mM DTT, 1 mM EDTA and 20% v/v glycerol.

Overproduction of DnaB(24–136) under control of the phage T7 ϕ10 promoter resulted in good yields of soluble protein, even following growth in minimal media. The yield of pure protein per litre of culture varied from 16 mg for 10%-^{13}C/u-^{15}N-labelled DnaB(24–136), to 45 mg for unlabelled DnaB(24–136).

Protein characterisation

The molecular weight of DnaB(24–136) and the extents of isotopic labelling of the proteins were determined by mass spectrometry. Samples at 0.5–1 g/l were extensively dialysed into 0.1% formic acid in water and analysed on a VG Quattro II mass spectrometer (VG Biotech Ltd) equipped with an electrospray ionisation source and a quadrupole-hexapole-quadrupole mass analyser. The molecular weight of DnaB(24–136) was confirmed to be 12,700 Da (calculated 12,701 Da), indicating that the terminal methionine had been processed in vivo. The extent of labelling of the proteins was determined to be 98% for both the u-^{15}N- and u-^{13}C/^{15}N-labelled DnaB(24–136).

Sequence alignments

Sequences were aligned using a BLASTP (version 2.0) gapped alignment procedure on the NCBI web page (http://www.ncbi.nlm.nih.gov/BLAST/). The program ALSCRIPT (version 2.03) [46] was used to prepare the plot of the sequence alignment.

Preparation of NMR samples

For the preparation of NMR samples, Pefabloc protease inhibitor (Boehringer) was added to the protein solutions at a concentration of 1 mM. The samples were subsequently ultrafiltered extensively using either an ultrafiltration cell equipped with a YM3 membrane (Amicon) or an Ultrafree-4 centrifugal filter unit equipped with a Biomax-5K membrane (Millipore). The final samples were prepared in 20 mM sodium phosphate buffer containing 1 mM EDTA and 0.02% w/v NaN_3 in 10% D_2O/90% H_2O at pH 7.5 or in 100% D_2O. Exchange of solvent from H_2O to D_2O was achieved by lyophilisation.

Residual dipolar couplings [47] were measured in solutions containing 20 mM phosphate buffer at pH 7.5 and a 5% w/v phospholipid mixture of DHPC (dihexanol phosphatidylcholine) and DMPC (dimyristoyl phosphatidylcholine) in a 1:3 molar ratio.

The affinity of DnaB(24–136) for Mg^{2+} was measured with a 0.8 mM sample of DnaB(24–136) in 20 mM sodium phosphate buffer at pH 7.5. The Mg^{2+} concentration was varied between 0 and 40 mM by addition of $MgCl_2$. Interaction with the dT_{16} single-stranded DNA fragment was probed using identical conditions, both in the presence and absence of 10 mM Mg^{2+}.

Affinities of DnaB(24–136) for ATP and DnaC were tested with a 0.3 mM sample of DnaB(24–136) in 10 mM TRIS-HCl buffer at pH 7.0, containing 2 mM DTT, 20 mM NaCl and 1 mM ATP in 10% D_2O/90% H_2O. A stock solution of DnaC was prepared using the same buffer. DnaC was titrated into the DnaB(24–136) sample and the sample volume readjusted to about 0.5 ml by ultrafiltration after each addition of DnaC.

NMR data collection

All NMR experiments were conducted at 32°C using Bruker DMX-600 or DRX-500 NMR spectrometers. Unless stated otherwise, measurements were made in 90% H_2O/10% D_2O. Spectra were processed using NMRPipe (version 1.6) [48] and analysed using ANSIG (version 3.3) [49].

Backbone resonance assignments were based on the assignments reported for DnaB(2–143) [31] and were confirmed and extended using 3D HNCA [50] and 3D NOESY-^{15}N-HSQC (τ_m = 60 ms) [51] spectra. Sidechain assignments were obtained primarily from 3D HC(C)H-TOCSY (D_2O), 3D H(C)CH-TOCSY (D_2O) [52] and 3D ^{13}C-HSQC-TOCSY (D_2O, τ_m = 16 ms) [53] spectra. A few additional sidechain resonances were assigned from NOESY spectra during the refinement procedure. In this way, sidechain ^{13}C and nonlabile ^{1}H resonances were assigned for all residues except R62, for which no assignments were obtained. Stereospecific assignments for isopropyl groups were obtained from a constant time 2D ^{13}C-HSQC spectrum recorded with the biosynthetically fractionally 10%-^{13}C/u-^{15}N-labelled protein sample [54].

Upper distance limits were collected from three different NOESY spectra – NOESY-^{15}N-HSQC (τ_m = 40 ms) [51], NOESY-^{13}C-HSQC (D_2O, τ_m = 50 ms) and NOESY-^{13}C-HSQC (optimised for aromatic residues, τ_m = 40 ms) [55]. A ^{13}C-HSQC-NOESY [56] spectrum was used to resolve assignment ambiguities in the NOESY-^{15}N-HSQC spectrum. $^3J_{HNH\alpha}$ coupling constants were measured in a 3D HNHA spectrum [57]. $^3J_{HNH\beta}$ and $^3J_{H\alpha H\beta}$ coupling constants were qualitatively measured in a 3D SG-TROSY-HNHB spectrum [32] and the 3D ^{13}C-HSQC-TOCSY

Table 1

Structural statistics for the NMR structure of DnaB(24–136).

Parameter	Value
Assigned NOE cross peaks	2463
Non-redundant NOE upper-distance limits	1194
Stereospecific assignments	67
Scalar coupling constants*	225
Dihedral-angle restraints	262
Residual dipolar coupling constants	84
AMBER-energy (kcal/mol)	–4350 ± 90
Residual NOE-restraint violations (Å)	
Sum	9.2 ± 0.4
Maximum	0.10 ± 0.00
Residual dihedral-angle restraint violations (°)	
Sum	23.8 ± 2.4
Maximum	1.9 ± 0.2
Rmsd†‡ (Å)	
Backbone atoms N, Cα, C′	0.51 ± 0.09
All heavy atoms	0.95 ± 0.09
Ramachandran plot appearance‡§	
most favoured regions (%)	90.6
additionally allowed regions (%)	8.4
generously allowed regions (%)	0.5
disallowed regions (%)	0.5

*88 $^{3}J(HN,H^{\alpha})$, 74 $^{3}J(N,H^{\beta})$, 30 $^{3}J(H^{\alpha},H^{\beta})$, 33 $^{1}J(H^{\alpha},C^{\alpha})$. †To the mean structure. ‡Residues 29–134. §From PROCHECK-NMR [69].

spectrum, respectively. A 3D α/β-HACACO spectrum was used to measure $^{1}J_{H\alpha C\alpha}$ coupling constants [58]. 2D α/β-HSQC spectra [58,59] were used to measure residual dipolar couplings between N and H^{N} at 0.1 mM and 1.0 mM protein concentration. Rapidly exchanging amide protons were identified in a 2D ROE-relayed-^{15}N-HSQC [60] spectrum employing selective excitation of the water resonance [61].

Binding of DnaC, single-stranded DNA, ATP or Mg^{2+} was monitored by ^{15}N-TROSY spectra [32,62,63]. Binding of DnaC was probed with 0.5:1, 1:1 and 1:2 (mol:mol) mixtures of DnaB(24–136) and DnaC.

Structure calculations

The NMR structure was calculated using the program DYANA (version 1.5) and the associated routines CALIBA, HABAS and GLOMSA [64]. In addition to scalar coupling constants, short range NOEs and Cα chemical shifts were used to generate restraints for ϕ, ψ and χ_1. $^{1}J_{H\alpha C\alpha}$ couplings deviating by more than +5 Hz from the random coil values were translated into ψ angle restraints of -47 ± 20^{o} [65]. One hundred random conformers were annealed in 10,000 steps using torsion-angle dynamics. The fifty conformers with the lowest residual restraint violations were minimised further, including also orientational restraints from residual dipolar couplings, using a variable target function algorithm [64,66]. The magnitude and rhombicity of the alignment tensor were estimated using the method of Clore *et al*. [67]. Finally, the twenty conformers with the lowest residual constraint violations were energy minimised with a 6 Å layer of explicit water using the program OPAL (version 2.6) [68].

Table 1 shows an overview of the structural statistics. The Ramachandran plot was analyzed using PROCHECK-NMR (version 3.4) [69]. For residues 29–134, all outliers correspond to residues in the segments with a low density of NMR restraints and no ϕ, ψ pair was found in forbidden regions for all twenty final conformers.

Secondary-structure elements and rmsd values were calculated using the program MOLMOL (version 2.6) [70]. A residue was determined to be in a particular regular secondary-structure motif if it was found in that conformation in more than half of the energy-minimised conformers. MOLMOL was also used to generate all molecular graphics figures.

Accession numbers

The coordinates of the twenty energy-refined DYANA conformers of the N-terminal domain of *E. coli* DnaB, together with the complete lists of NMR-derived structural restraints have been deposited in the Brookhaven Protein Data Bank with the accession code 1JWE. The NMR chemical shifts have been deposited at the BioMagResBank (BMRB) under the accession code 4297.

Acknowledgements

We thank Carl Braybrook (Australian National University) for performing the mass spectrometry and Jackie Wilce (University of Sydney) for performing the analytical ultracentrifugation. Financial support from the Australian Research Council, the Australian Department of Industry, Science and Tourism, the Australian National University, the Swedish Natural Science Research Council, and the Erik and Edith Fernström Foundation for Medical Research are gratefully acknowledged.

References

1. Matson, S.W., Bean, D.W. & George, J.W. (1994). DNA helicases: enzymes with essential roles in all aspects of DNA metabolism. *BioEssays* **16**, 13-22.
2. Lohman, T.M. & Bjornson, K.P. (1996). Mechanisms of helicase-catalyzed DNA unwinding. *Annu. Rev. Biochem.* **65**, 169-214.
3. Ellis, N.A. (1997). DNA helicases in inherited human disorders. *Curr. Opin. Gen. Develop.* **7**, 354-363.
4. Subramanya, H.S., Bird, L.E., Brannigan, J.A. & Wigley, D.B. (1996). Crystal structure of a DExx box DNA helicase. *Nature* **384**, 379-383.
5. Yao, N.H., *et al.*, & Weber, P. C. (1997). Structure of the hepatitis C virus RNA helicase domain. *Nat. Struct. Biol.* **4**, 463-467.
6. Korolev, S., Hsieh, J., Gauss, G.H., Lohman, T.M. & Waksman, G. (1997). Major domain swiveling revealed by the crystal structures of complexes of *E.coli* Rep helicase bound to single-stranded DNA and ADP. *Cell* **90**, 635-647.
7. Kim, J.L., *et al.*, & Caron, P.R. (1998). Hepatitis C virus NS3 RNA helicase domain with a bound oligonucleotide: the crystal structure provides insights into the mode of unwinding. *Structure* **6**, 89-100.
8. Bird, L.E., Subramanya, H.S. & Wigley, D.B. (1998). Helicases: a unifying structural theme? *Curr. Opin. Struct. Biol.* **8**, 14-18.
9. Röleke, D., *et al.*, & Saenger, W. (1997). Crystallization and preliminary X-ray crystallographic and electron microscopic study of a bacterial DNA helicase (RSF1010 *RepA*). *Acta Crystallogr. D* **53**, 213-216.
10. Bird, L.E., Håkansson, K., Pan, H. & Wigley, D.B. (1997). Characterization and crystallization of the helicase domain of bacteriophage T7 gene 4 protein. *Nucleic Acids Res.* **25**, 2620-2626.
11. Briercheck, D.M., Wood, T.C., Allison, T.J., Richardson, J.P. & Rule, G.S. (1998). The NMR structure of the RNA binding domain of *E. coli* rho factor suggests possible RNA-protein interactions. *Nat. Struct. Biol.* **5**, 393-399.
12. Allison, T.J., Wood, T.C., Briercheck, D.M., Rastinejad, F., Richardson, J.P. & Rule, G.S. (1998). Crystal structure of the RNA-binding domain from transcription termination factor rho. *Nat. Struct. Biol.* **5**, 352-356.
13. Arai, K. & Kornberg, A. (1981). Mechanism of *dnaB* protein action III. Allosteric roles of ATP in the alteration of DNA structure by *dnaB* protein in priming replication. *J. Biol. Chem.* **256**, 5260-5266.
14. Kornberg, A. & Baker, T.A. (1991). *DNA replication* (2nd edn). W.H. Freeman, New York.
15. Funnell, B.E., Baker, T.A. & Kornberg, A. (1987). *In vitro* assembly of a prepriming complex at the origin of the *Escherichia coli* chromosome. *J. Biol. Chem.* **262**, 10327-10334.
16. Sekimuzu, K., Bramhill, D. & Kornberg, A. (1988). Sequential early stages in the *in vitro* initiation of replication at the origin of the *Escherichia coli* chromosome. *J. Biol. Chem.* **263**, 7124-7130.
17. Marszalek, J. & Kaguni, J.M. (1994). DnaA protein directs the binding of DnaB protein in initiation of DNA replication in *Escherichia coli*. *J. Biol. Chem.* **269**, 4883-4890.
18. LeBowitz, J.H. & McMacken, R. (1986). The *Escherichia coli dnaB* replication protein is a DNA helicase. *J. Biol. Chem.* **261**, 4738-4748.
19. Arai, K. & Kornberg, A. (1981). Mechanism of *dnaB* protein action. II. ATP hydrolysis by *dnaB* protein dependent on single- or double-stranded DNA. *J. Biol. Chem.* **256**, 5253-5259.
20. Wickner, S. & Hurwitz, J. (1975). Interaction of *Escherichia coli dnaB* and *dnaC(D)* gene products *in vitro*. *Proc. Natl Acad. Sci. USA* **72**, 921-925.
21. Tougu, K., Peng, H. & Marians, K.J. (1994). Identification of a domain of *Escherichia coli* primase required for functional interaction with the DnaB helicase at the replication fork. *J. Biol. Chem.* **269**, 4675-4682.

22. Kim, S., Dallman, H.G., McHenry, C.S. & Marians, K.J. (1996). Coupling of a replicative polymerase and helicase: a τ-DnaB interaction mediated rapid replication fork movement. *Cell* 84, 643-650.
23. Bujalowski, W., Klonowska, M.M. & Jezewska, M.J. (1994). Oligomeric structure of *Escherichia coli* primary replicative helicase DnaB protein. *J. Biol. Chem.* 269, 31350-31358.
24. Nakayama, N., Arai, N., Kaziro, Y. & Arai, K. (1984). Structural and functional studies of the *dnaB* protein using limited proteolysis. Characterization of domains for DNA-dependent ATP hydrolysis and for protein association in the primosome. *J. Biol. Chem.* 259, 88-96.
25. Biswas, S.B., Chen, P.-H. & Biswas, E.E. (1994). Structure and function of *Escherichia coli* DnaB protein: Role of the N-terminal domain in helicase activity. *Biochemistry* 33, 11307-11314.
26. San Martin, M.C., Stamford, N.P.J., Dammerova, N., Dixon, N.E. & Carazo, J.M. (1995). A structural model for the *Escherichia coli* DnaB helicase based on electron microscopy data. *J. Struct. Biol.* 114, 167-176.
27. Yu, X., Jezewska, M.J., Bujalowski, W. & Egelman, E.H. (1996). The hexameric *E. coli* DnaB helicase can exist in different quarternary states. *J. Mol. Biol.* 259, 7-14.
28. San Martin, C., *et al.*, & Carazo, J. M. (1998). Three-dimensional reconstructions from cryoelectron microscopy images reveal an intimate complex between helicase DnaB and its loading partner DnaC. *Structure* 6, 501-509.
29. Egelman, E.H. (1996). Homomorphous hexameric helicases: tales from the ring cycle. *Structure* 4, 759-762.
30. Miles, C.S., Weigelt, J., Stamford, N.P.J., Dammerova, N., Otting, G. & Dixon, N.E. (1997). Precise limits of the N-terminal domain of DnaB helicase determined by NMR spectroscopy. *Biochem. Biophys. Res. Commun.* 231, 126-130.
31. Weigelt, J., Miles, C.S., Dixon, N.E. & Otting, G. (1998). Backbone NMR assignments and secondary structure of the N-terminal domain of DnaB helicase from *E. coli*. *J. Biomol. NMR* 11, 233-234.
32. Weigelt, J. (1998). Single scan, sensitivity- and gradient-enhanced TROSY for multidimensional NMR experiments. *J. Am. Chem. Soc.* 120, 10778-10779.
33. Otting, G. & Wüthrich, K. (1990). Heteronuclear filters in two-dimensional [^{1}H,^{1}H]-NMR spectroscopy: combined use with isotope labeling for studies of macromolecular conformation and intermolecular interactions. *Quart. Rev. Biophys.* 23, 39-96.
34. Zwahlen, C., Legault, P., Vincent, S.J.F., Greenblatt, J., Konrat, R. & Kay, L.E. (1997). Methods for measurement of intermolecular NOEs by multinuclear NMR spectroscopy: Application to a bacteriophage λ N-Peptide/*boxB* RNA complex. *J. Am. Chem. Soc.* 119, 6711-6721.
35. Barth, A., Frost, K., Wahab, M., Brandt, W., Schlader, H.D. & Franke, R. (1994). Classification of serine proteases derived from steric comparisons of their active site geometry, part II: Ser, His, Asp arrangements in proteolytic and non-proteolytic proteins. *Drug Des. Discov.* 12, 89-111.
36. Nakayama, N., Arai, N., Bond, M.W., Kaziro, Y. & Arai, K. (1984). Nucleotide sequence of *dnaB* and the primary structure of the *dnaB* protein from *Escherichia coli*. *J. Biol. Chem.* 259, 97-101.
37. Maurer, R. & Wong, A. (1988). Dominant lethal mutations in the *dnaB* helicase gene of *Salmonella typhimurium*. *J. Bacteriol.* 170, 3682-3688.
38. Stordal, L. & Maurer, R. (1996). Defects in general priming conferred by linker region mutants of *Escherichia coli dnaB*. *J. Bacteriol.* 178, 4620-4627.
39. Holm, L. & Sander, C. (1993). Protein structure comparison by alignment of distance matrices. *J. Mol. Biol.* 233, 123-138.
40. Morais Cabral, J.H., Jackson, A.P., Smith, C.V., Shikotra, N., Maxwell, A. & Liddington, R.C. (1997). Crystal structure of the breakage-reunion domain of DNA gyrase. *Nature* 388, 903-906.
41. Berger, J.M., Gamblin, S.J., Harrison, S.C. & Wang, J.C. (1996). Structure and mechanism of DNA topoisomerase II. *Nature* 379, 225-232.
42. Yu, X. & Egelman, E.H. (1997). The RecA hexamer is a structural homologue of ring helicases. *Nat. Struct. Biol.* 4, 101-104.
43. Studier, F.W., Rosenberg, A.H., Dunn, J.J. & Dubendorff, J.W. (1990). Use of T7 RNA polymerase to direct expression of cloned genes. *Methods Enzymol.* 185, 60-89.
44. Leiting, B., De Francesco, R., Cortese, R., Otting, G. & Wüthrich, K. (1993). The three-dimensional NMR-solution structure of the polypeptide fragment 195-286 of the LFB1/HNF1 transcription factor from rat liver comprises a non-classical homeodomain. *EMBO J.* 12, 1797-1803.
45. Stamford, N.P.J. (1992). PhD thesis. Proteins of the *E. coli* replisome. Australian National University, Canberra.
46. Barton, G.J. (1993). ALSCRIPT a tool to format multiple sequence alignments. *Prot. Eng.* 6, 37-40.
47. Tjandra, N. & Bax, A. (1997). Direct measurement of distances and angles in biomolecules by NMR in a dilute liquid crystalline medium. *Science* 278, 1111-1114.
48. Delaglio, F., Grzesiek, S., Vuister, G.W., Zhu, G., Pfeifer, J. & Bax, A. (1995). NMRPipe: A multidimensional spectral processing system based on UNIX pipes. *J. Biomol. NMR* 6, 277-293.
49. Kraulis, P.J., Domaille, P.J., Campbell-Burk, S.L., van Aken, T. & Laue, E.D. (1994). Solution structure and dynamics of Ras p21.GDP determined by heteronuclear three- and four-dimensional NMR spectroscopy. *Biochemistry* 33, 3515-3531.
50. Grzesiek, S. & Bax, A. (1992). Improved 3D triple-resonance NMR techniques applied to a 31 kDa protein. *J. Magn. Res.* 96, 432-440.
51. Talluri, S. & Wagner, G. (1996). An optimized 3D NOESY-HSQC. *J. Magn. Res. B* 112, 200-205.
52. Wang, H. & Zuiderweg, E.R.P. (1995). HCCH-TOCSY spectroscopy of ^{13}C-labeled proteins in H_2O using heteronuclear cross-polarization and pulsed-field gradients. *J. Biomol. NMR* 5, 207-211.
53. Xu, R.X., Olejniczak, E.T. & Fesik, S.W. (1992). Stereospecific assignments and χ_1 rotamers for FKBP when bound to ascomycin from ^3JHα,Hβ and ^3JHN,Hβ coupling constants. *FEBS Lett.* 305, 137-143.
54. Szyperski, T., Neri, D., Leiting, B., Otting, G. & Wüthrich, K. (1992). Support of ^{1}H NMR assignments in proteins by biosynthetically directed fractional ^{13}C-labeling. *J. Biomol. NMR* 2, 323-334.
55. Zuiderweg, E.R.P. & Fesik, S.W. (1989). Heteronuclear three-dimensional NMR spectroscopy of the inflammatory protein C5a. *Biochemistry* 28, 2387-2391.
56. Fesik, S.W. & Zuiderweg, E.R.P. (1988). Heteronuclear three-dimenesional NMR spectroscopy. A strategy for the simplification of homonuclear two-dimensional NMR spectra. *J. Magn. Res.* 78, 588-593.
57. Vuister, G.W. & Bax, A. (1993). Quantitative *J* correlation: A new approach for measuring homonuclear three-bond $J(H^NH^\alpha)$ coupling constants in ^{15}N-enriched proteins. *J. Am. Chem. Soc.* 115, 7772-7777.
58. Andersson, P., Weigelt, J. & Otting, G. (1998). Spin-state selection filters for the measurement of heteronuclear one-bond coupling constants. *J. Biomol. NMR* 12, 435-441.
59. Wang, Y.-X., *et al.*, & Bax, A. (1998). Simultaneous measurement of ^{1}H-^{15}N, ^{1}H-^{13}C′, and ^{15}N-^{13}C′ dipolar couplings in a perdeuterated 30 kDa protein dissolved in a dilute liquid crystalline phase. *J. Am. Chem. Soc.* 120, 7385-7386.
60. Grzesiek, S. & Bax, A. (1993). Measurement of amide proton exchange proton exchange rates and NOEs with water in ^{13}C/^{15}N-enriched calcineurin B. *J. Biomol. NMR* 3, 627-638.
61. Liepinsh, E. & Otting, G. (1999). Water-protein NOEs: optimized scheme for selective water excitation. *J. Biomol. NMR*, 13, 73-76.
62. Pervushin, K.V., Wider, G. & Wüthrich, K. (1998). Single transition-to-single transition polarization transfer (ST2-PT) in [^{15}N,^{1}H]-TROSY. *J. Biomol. NMR* 12, 345-348.
63. Czisch, M. & Boelens, R. (1998). Sensitivity enhancement in the TROSY experiment. *J. Magn. Res.* 134, 158-160.
64. Güntert, P., Mumenthaler, C. & Wüthrich, K. (1997). Torsion angle dynamics for NMR structure calculation with the new program DYANA. *J. Mol. Biol.* 273, 283-298.
65. Vuister, G.W., Delaglio, F. & Bax, A. (1993). The use of $^1J_{C\alpha H\alpha}$ coupling constants as a probe for protein backbone conformation. *J. Biomol. NMR* 3, 67-80.
66. Güntert, P., Braun, W. & Wüthrich, K. (1991). Efficient computation of three-dimensional protein structures in solution from nuclear magnetic resonance data using the program DIANA and the supporting programs CALIBA, HABAS and GLOMSA. *J. Mol. Biol.* 217, 517-530.
67. Clore, G.M., Gronenborn, A.M. & Bax, A. (1998). A robust method for determining the magnitude of the fully asymmetric alignment tensor of oriented macromolecules in the absence of structural information. *J. Magn. Res.* 133, 216-221.
68. Luginbühl, P., Güntert, P., Billeter, M. & Wüthrich, K. (1996). The new program OPAL for molecular dynamics simulations and energy refinements of biological macromolecules. *J. Biomol. NMR* 8, 136-146.
69. Laskowski, R.A., Rullmann, J.A.C., MacArthur, M.W., Kaptein, R. & Thornton, J.M. (1996). AQUA and PROCHECK-NMR: programs for checking the quality of protein structures solved by NMR. *J. Biomol. NMR* 8, 477-486.
70. Koradi, R., Billeter, M. & Wüthrich, K. (1996). MOLMOL: a program for display and analysis of macromolecular structures. *J. Mol. Graph.* 14, 51-55.
71. Sevilla-Sierra, P., Otting, G. & Wüthrich, K. (1994). Determination of the nuclear magnetic resonance structure of the DNA-binding domain of the P22 c2 repressor(1-76) in solution and comparison with the DNA binding domain of the 434 repressor. *J. Mol. Biol.* 235, 1003-1020.